THE JOURNAL OF PHYSICAL CHEMISTRY B

Article

pubs.acs.org/JPCB

Rotational and Translational Dynamics of Rhodamine 6G in a Pyrrolidinium Ionic Liquid: A Combined Time-Resolved Fluorescence Anisotropy Decay and NMR Study

Jianchang Guo,[†] Kee Sung Han,[†] Shannon M. Mahurin,[†] Gary A. Baker,[‡] Patrick C. Hillesheim,[†] Sheng Dai,[†] Edward W. Hagaman,*[,†] and Robert W. Shaw*[,†]

[†]Chemical Sciences Division, Oak Ridge National Laboratory, Oak Ridge, Tennessee 37831, United States

[‡]Department of Chemistry, University of Missouri—Columbia, Columbia, Missouri 65211, United States

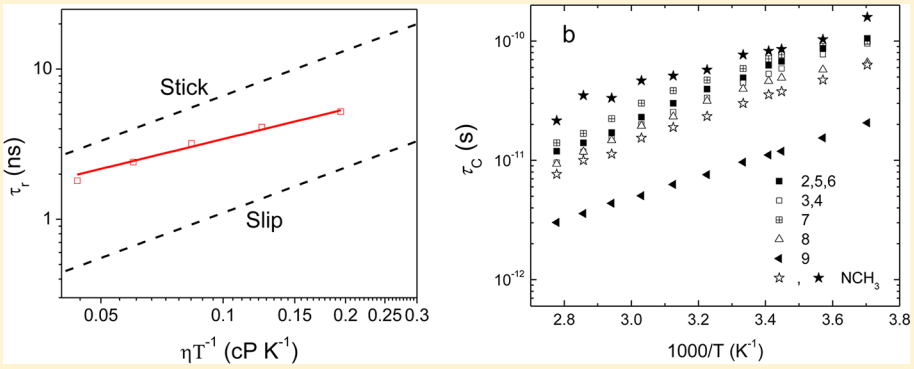

ABSTRACT: NMR spectroscopy and time-resolved fluorescence anisotropy decay (TRFAD) are two of the most commonly used methods to study solute−solvent interactions. However, only a few studies have been reported to date using a combined NMR and TRFAD approach to systematically investigate the overall picture of diffusional and rotational dynamics of both the solute and solvent. In this paper, we combined NMR and TRFAD to probe fluorescent rhodamine dye in a pyrrolidinium-based room temperature ionic liquid (RTIL), an emergent environmentally friendly solvent type used in several energy-related applications. A specific interaction of the R6G cation and $[Tf_2N]$ anion was identified, resulting in near-stick boundary condition rotation of R6G in this RTIL. The diffusional rates of the R6G solute and $[C_4mpyr][Tf_2N]$ solvent derived from ^1H NMR suggest the rates are proportional to their corresponding hydrodynamic radii. The ^1H and ^{13}C NMR studies of self-rotational dynamics of $[C_4mpyr][Tf_2N]$ showed that the self-rotational correlation time of $[C_4mpyr]^+$ is 47 ± 2 ps at 300 K. At the same temperature, we find that the correlation time for N−CH_3 rotation in $[C_4mpyr]^+$ is 77 ± 2 ps, comparable to overall molecular reorientation. This slow motion is attributed to properties of the cation structure.

INTRODUCTION

Room temperature ionic liquids (RTILs) are molten salts at ambient conditions, typically consisting of a delocalized organic cation and an anion forming a liquid at room temperature. RTILs have been used in many energy-related applications, including separations and catalysis, due to their desirable properties: negligible volatility, high electrochemical and thermal stability, and high ionic conductivity.[1−8] In spite of broad interest in RTILs, their microscopic dynamics have only just recently begun to receive attention.[9−21] A deeper understanding of the microscopic dynamics and the related physicochemical properties of RTILs is warranted to optimize future applications. Investigation of solute−solvent interactions can provide critical information concerning intermolecular interactions, solvation modes, and related phenomena.[22] These interactions play a central role in chemical reactions, solute transport, separations, and catalysis. Although a wealth of information is available concerning the rotational dynamics of small molecules in conventional solvents, studies of rotational dynamics of solutes in RTILs are sparse.[15,21,23−27] The hybrid organic−ionic nature of RTILs and the interplay between different forces can lead to complex intermolecular interactions. Integration of results from complementary experimental techniques is expected to provide new insight into RTIL dynamics.

Among a variety of techniques used to study the rotational dynamics, time-resolved fluorescence anisotropy decay (TRFAD) and nuclear magnetic resonance (NMR) spin−lattice relaxation measurements are the most valuable experimental methods.[28,29] Although NMR has been used regularly to understand the translational and rotational diffusion dynamics of ionic liquids themselves, the rotational and translational dynamics of dilute solutes in RTILs have been addressed less frequently using NMR, possibly due to signal-to-

Received: April 3, 2012
Revised: June 8, 2012
Published: June 12, 2012

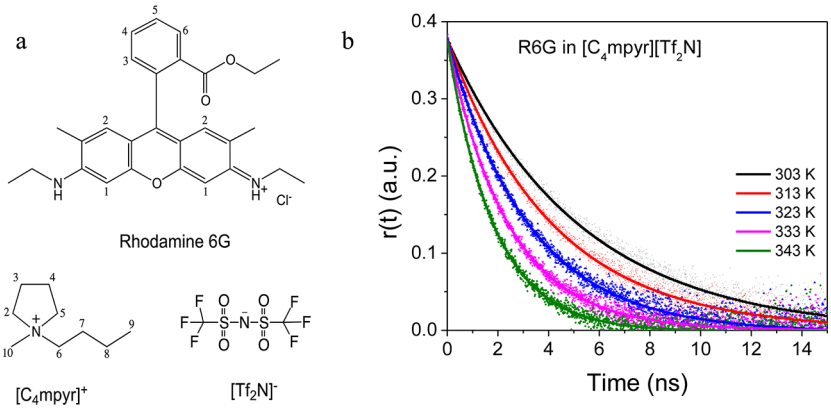

Figure 1. (a) Molecular structures and numbering for R6G and $[C_4mpyr][Tf_2N]$. (b) Normalized fluorescence anisotropy decay for 2 μM R6G in $[C_4mpyr][Tf_2N]$ at different temperatures. The solid lines are single-exponential fits to the data points.

noise limitations. On the other hand, TRFAD has been used by many researchers to study the rotational diffusion as well as solvation dynamics of solutes in RTILs.[10,13−15,17−19,21,30−35] In those studies, nonspecific interactions, such as dipole−dipole and van der Waals interactions, as well as specific interactions, such as hydrogen-bonding, have been used to describe the solute−solvent interactions. Most reported investigations have used neutral solutes, except a few studies in recent years.[21,30−32] The effect of charged solutes on rotational dynamics is not clearly understood.

In this paper, we combine TRFAD and NMR to investigate model charged solute rotational and translational diffusion dynamics toward elucidating the solute−solvent intermolecular interactions in RTILs. Positively charged Rhodamine 6G (R6G) was selected as solute and *N*-butyl-*N*-methylpyrrolidinium bis(trifluoromethylsulfonyl)imide $[C_4mpyr][Tf_2N]$ was selected as solvent. The molecular structures of $[C_4mpyr][Tf_2N]$ and R6G are shown in Figure 1a. The rotational dynamics of R6G in $[C_4mpyr][Tf_2N]$ were measured at different temperatures using TRFAD. The self-diffusion and self-rotation dynamics of $[C_4mpyr]^+$ were obtained through NMR spectroscopy. The effect of solute−solvent interaction on both rotational and translational diffusion dynamics is discussed.

EXPERIMENTAL SECTION

Material Synthesis and Sample Preparation. Spectroscopy-grade $[C_4mpyr][Tf_2N]$ was synthesized following modifications to a reported procedure.[36] In short, all starting heterocycles and alkylhalides were doubly or triply distilled before RTIL synthesis in order to reduce their optical emission background. The halide salts required multiple recrystallizations to remove traces of color and luminescent impurities. No discernible differences have been noted in the $^1H/^{13}C$ NMR spectra, pointing to the low levels of chromophore/luminophore contamination. Inert atmospheres, careful control of temperature, and protection from light were implemented for all syntheses. The viscosity of $[C_4mpyr][Tf_2N]$ is 74.4 cP at 298 K.

To prepare a given sample of rhodamine 6G (Molecular Probes) in $[C_4mpyr][Tf_2N]$ for TRFAD experiments, a small volume of 5×10^{-4} M ethanolic R6G stock solution was micropipeted into an appropriate volume of $[C_4mpyr][Tf_2N]$ to obtain a 2×10^{-6} M R6G concentration. The resulting solution was pumped under vacuum overnight and was then transferred into a 1 cm path length sample cuvette. For the NMR measurements a 5×10^{-2} (1×10^{-2}) M R6G solution was prepared by dissolving 48 (9.6) mg of R6G powder in 2 mL of $[C_4mpyr][Tf_2N]$. This mixture was placed in an ultrasonic bath for 90 min. A clear, dark red solution was obtained. This solution was pumped under vacuum at 383 K until a trace water resonance was no longer detected in the NMR spectrum.

Time-Resolved Fluorescence Anisotropy Decay (TRFAD). The time-resolved fluorescence anisotropy decay (TRFAD) apparatus consisted of a visible collinear optical parametric amplifier (OPA 9400, Coherent Lasers, Santa Clara, CA) pumped by a Ti:sapphire regenerative amplifier laser (RegA 9000, Coherent Lasers) at a 250 kHz repetition rate, along with a single photon counting detection setup. The output beam power from the amplifier was about 1.2 W, which was used to produce a wavelength tunable OPA output in the 490−700 nm spectral range. Excitation was at 532 nm with a 150 fs fwhm typical pulse duration and <8 nJ pulse energy. Fluorescence emission was selected by using a 10 nm fwhm bandpass filter centered at 575 nm. The detector includes an actively quenched single photon avalanche photodiode (PDM 50CT module, Micro Photon Devices) connected to time correlated single photon counting (TCSPC) electronics (PicoHarp 300, PicoQuant, Germany). The instrumental response time was ~40 ps.

Measurements of time-resolved fluorescence anisotropy, $r(t)$, involves collecting data for four polarization combinations of an excitation half-wave plate and an emission linear polarizer and calculating according the following relation:

$$r(t) = \frac{I_{VV}(t) - GI_{VH}(t)}{I_{VV}(t) + 2GI_{VH}(t)} \quad (1)$$

where $I_{VV}(t)$ and $I_{VH}(t)$ are the fluorescence decays measured with parallel and perpendicular polarizations relative to the vertical polarization excitation light, respectively. The G factor was obtained by measuring two additional decays, $I_{HV}(t)$ and $I_{HH}(t)$, and calculating $G = \int I_{HV}(t)\,dt / \int I_{HH}(t)\,dt$.

NMR Experiments. NMR measurements were performed using a 9.4 T Bruker Avance NMR spectrometer at Larmor frequencies of 400.1 and 100.6 MHz for ^1H and ^{13}C, respectively. The sample temperature was controlled by use of a resistance heater in the 5 mm Z-grad probe using air for the heat transfer gas for high temperatures and N_2 gas evaporated directly from a liquid nitrogen dewar for low temperatures.

dx.doi.org/10.1021/jp303186v | J. Phys. Chem. B 2012, 116, 7883−7890

Temperature calibration was performed with 100% ethylene glycol and 100% methanol for temperatures above and below 300 K, respectively, according to the Bruker temperature calibration manual. Chemical shifts are reported with respect to external TMS: δ = 0 ppm.

The self-diffusion coefficients, D, of the [C_4mpyr] cation and R6G (5×10^{-2} M in [C_4mpyr][Tf_2N]) were measured using ^{1}H pulsed-field gradient nuclear magnetic resonance (PFG-NMR) spectroscopy as a function of temperature. A stimulated echo bipolar pulse-gradient pulse (stebpgp) sequence was used for the determination of D. The echo heights were recorded as a function of the strength of the gradient pulse, g, incremented in 16 equal intervals from 2 to 95% of the maximum gradient pulse strength (54.4 ± 0.3 G/cm). The echo heights were fit to $S(g) = S(0)\exp[-D\gamma^2\delta^2g^2(\Delta - \delta/3)]$, where $S(g)$ and $S(0)$ are the echo height at the gradient strength g and 0, respectively, γ is the gyromagnetic ratio of the proton, δ is gradient pulse length, and Δ is the duration between the two gradient pulses.[37] Convection effects induced by a temperature gradient in the sample were minimized by restricting the sample length along the z axis to 1 mm using a Shigemi sample tube[38] and fixing δ to 16 ms and adjusting Δ to obtain well-characterized echo decays.

^{1}H and ^{13}C spin−lattice relaxation data were acquired as a function of temperature using an inversion recovery pulse sequence.[39] The rotational correlation times, τ_c, at each resolved site of the cation of [C_4mpyr][Tf_2N] were calculated from ^{1}H and ^{13}C T_1 data, independently. The ^{1}H T_1 data were fit to the Bloembergen−Purcell−Pound (BPP) equation[40]

$$\frac{1}{T} = \frac{6}{5}\frac{\gamma^4\hbar^2}{b^6}I(I+1)\left[\frac{\tau_c}{1+\omega_0^2\tau_c^2} + \frac{4\tau_c}{1+4\omega_0^2\tau_c^2}\right] \quad (2)$$

where γ is the gyromagnetic ratio of the proton (2π·42.576 MHz/Tesla), $\hbar$ is reduced Plancks constant, b (= Σr) is the distance between protons and the sum runs over all protons that are dipolar coupled to the proton evaluated, I is nuclear spin number of the proton (= 1/2), $\omega_0 = 2\pi\nu_0$, where ν_0 is 400.1 MHz at 9.4 T, the proton observation frequency, and τ_c is the rotational correlation time. Equation 2 is derived under the isotropic motion approximation and applies in the extreme narrowing limit ($T_1 = T_2$). Where a minimum is observed in plots of T_1 vs temperature, $\omega_0\tau_c = 0.616$, τ_c is 2.45×10^{-10} s/rad, and the distance term, b, can be calculated as the only unknown in eq 2.[40] The distance term is assumed constant as a function of temperature and used to calculate τ_c from T_1 data taken at different temperatures. The T_1 minimum, (T_{1min}), occurs at the temperature where the optimum coupling of the spin manifold and the lattice motions is achieved. At this point the T_1 value is largely determined by the strength of the dipolar interaction at the proton site. Relative T_1 values are valuable indicators of the dipolar coupling strength at each proton site.

The ^{1}H−^{13}C dipole−dipole interaction is the dominant spin−lattice relaxation mechanism for ^{13}C nuclei that are directly bonded to hydrogen. The equation for spin−lattice relaxation by heteronuclear dipolar relaxation can be written as[41]

$$\frac{1}{T_1} = \frac{N}{10}\frac{\gamma_H^2\gamma_C^2\hbar^2}{r^6}\left[\frac{\tau_c}{1+(\omega_H-\omega_c)^2\tau_c^2} + \frac{3\tau_c}{1+\omega_c^2\tau_c^2} + \frac{6\tau_c}{1+(\omega_H+\omega_c)^2\tau_c^2}\right] \quad (3)$$

where N is the number of protons directly bonded to carbon, γ_H and γ_C are the gyromagnetic ratio of the proton and the carbon, respectively, r is the distance between the carbon and the proton (1.09 Å), ω_H and ω_C are the angular NMR frequencies of the proton and the carbon, respectively, and τ_C is the effective correlation time for molecular reorientation. Except as otherwise noted, the correlation times referred to in this work are those derived from eqs 2 and 3.

RESULTS AND DISCUSSION

The normalized fluorescence anisotropy decays of R6G in [C_4mpyr][Tf_2N] at different temperatures are shown Figure 1b. The decay times decrease with increasing temperature, consistent with the observed lower viscosity at higher temperature. The anisotropy decay at each temperature can be suitably fit using a single exponential function. Many studies have found acceptable fitting of rotational dynamics of dyes in RTILs using a single exponential.[30−32,35,42] Other studies found that multiexponential decay fits were superior to single exponential or stretch exponential fitting.[43,44] Funston et al[44] reported on Coumarin 153 (C153) in the same ionic liquid studied here and employed multiexponential fitting. Also note that Das and Sarkar[42] very recently measured diffusion coefficients for C153, but in imidazolium alkyl sulfate ionic liquids. Carlson et al[43] reported on C153 in 1-hydroxyethyl-4-amino-1,2,4-triazolium nitrate RTIL and used multiexponential fitting. The purity of the RTIL solvent, especially the residual water content, can play a role in the local environment heterogeneity and thus the diffusion complexity. In addition the particular dye examined and its ionic (R6G) vs neutral (C153) character will affect diffusion kinetics.

The decay time, τ_r, decreased from 5.2 to 1.8 ns as the temperature increased from 303 to 343 K. The experimentally measured rotation times can be analyzed within the framework of the Stokes−Einstein−Debye (SED) hydrodynamic theory. According to this theory, the rotation time is related to the macroscopic viscosity, η, by

$$\tau_r = \frac{\eta VfC}{kT} \quad (4)$$

where V is the van der Waals volume of the solute, C is the boundary condition parameter, which has values between 0 and 1, and f is the shape factor introduced to account for nonspherical solute molecules, usually treated as either symmetric or asymmetric ellipsoids and having a value greater than 1.

To calculate the reorientation time of R6G using the SED theory, the van der Waals volume for the R6G cation was estimated using Edward's increment method[45] and found to be 414 Å^3. R6G was modeled as an ellipsoid and the largest dimension as calculated from molecular simulation was taken as the long axis ($2a$); the short-in-plane axis ($2b$) was taken from the dimension perpendicular to $2a$, and the thickness of aromatic rings ($2c$) was calculated from the relation $V = (4\pi/3)abc$ as the phenyl ring is oriented orthogonally to the xanthenyl moiety. The three axis radii, a, b, and c from above treatment

dx.doi.org/10.1021/jp303186v | J. Phys. Chem. B 2012, 116, 7883−7890

are 7.8, 7.0, and 1.8 Å, respectively. The diffusion coefficients D_i were calculated using the Einstein relation with ζ_i as the friction coefficient along the three principal axes of rotation

$$D_i = \frac{kT}{\zeta_i} \tag{5}$$

The reorientation times can be calculated by using eq 6 if the anisotropy decay can be fit using a single exponential, the absorption and emission dipoles are parallel, and the direction of the transition dipole coincides with the long axis (a).[33]

$$\tau_r = \frac{1}{12}\left(\frac{4D_a + D_b + D_c}{D_aD_b + D_bD_c + D_cD_a}\right) \tag{6}$$

D_a, D_b, and D_c are the diffusion coefficients along the a, b, and c axes, respectively. For R6G, we assume that this condition is fulfilled.

The friction coefficients ζ_i for an asymmetric ellipsoid with a slip boundary condition were obtained from numerically tabulated values of Sension and Hochstrasser[46] assuming that the dimensionless friction coefficients vary linearly from the tabulated values. The friction coefficients for an asymmetric ellipsoid with a stick boundary condition were obtained from numerically tabulated values of Small and Isenberg.[47] Figure 2

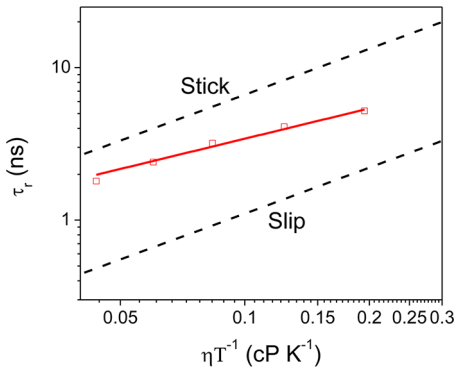

Figure 2. Plot of the reorientation times, τ_r, versus η/T for R6G in [C_4mpyr][Tf_2N]. The solid line passing through the data points was obtained by performing a least-squares fit. Theoretically calculated reorientation times using SED theory along with slip (lower dashed-line) and slick (upper dashed-line) boundary conditions are shown in the figure.

shows the theoretical slip (lower dashed line) and stick (upper dashed line) boundary conditions for R6G in [C_4mpyr][Tf_2N]. From the calculated τ_r the shape factor with a stick boundary condition can be obtained using eq 1 with $C_{stick} = 1$. C_{slip} and f were obtained by taking the ratio of $\tau_r^{slip}/\tau_r^{stick}$. Hence, the values of C_{slip} and f for R6G are 0.25 and 1.68, respectively. The data points are experimentally measured reorientation times at different η/T. A glance at the figure reveals that the rotational dynamics of R6G lie intermediate between slip and stick boundary conditions but closer to the stick boundary condition. A least-squares analysis of the data produces $\tau_r = (15.6 \pm 1.5)(\eta/T)^{0.66\pm0.05}$ ($N = 5$, $R = 0.983$). Here the N and R are the number of data points and regression coefficient, respectively. To better understand the solute−solvent interaction, the experimentally observed boundary condition parameters C_{obs} were calculated using eq 4. The averaged C_{obs} obtained at five different temperatures is 0.71. This value is almost three times C_{slip} and more closely approaches the stick boundary condition.

According to the SED theory, rotational diffusion of a solute molecule is solely governed by solvent viscosity in the absence of specific interactions, i.e., electrostatic force or hydrogen bonding. In such cases, the rotational dynamics follow slip hydrodynamics if the van der Waals volumes of solvent and solute are similar. For [C_4mpyr][Tf_2N], the van der Waals volume calculated from Edward's increment method is 332 Å^3 (in excellent agreement with the reported volume of 338 Å^3),[48] a magnitude 20% smaller than the 414 Å^3 volume calculated for R6G. The relative size effect can be rationalized by Gierer−Wirtz (GW) quasihydrodynamic theory.[21] According to GW theory, the friction coefficient C_{GW} can be expressed by a solvent volume V_s and probe solute volume V_p as

$$C_{GW} = \sigma C_0$$
$$\sigma = \frac{1}{1 + 6(V_S/V_P)^{1/3}C_0}$$
$$C_0 = \left[\frac{6(V_S/V_P)^{1/3}}{(1 + 3(V_S/V_P)^{1/3})^4} + \frac{1}{(1 + 4(V_S/V_P)^{1/3})^3}\right] \tag{7}$$

The boundary condition parameter C_{GW} for R6G/[C_4mpyr][Tf_2N] calculated from eq 7 is 0.0304, which is much smaller than observed friction coefficient C_{obs}, suggesting that a treatment that only considers the molecular size of solvent and solute molecules cannot explain the rotational dynamics of R6G in [C_4mpyr][Tf_2N]. This indicates that specific solute−solvent interactions may account for the near-stick rotational dynamics. Considering the positive charge of R6G and the ionic nature of [C_4mpyr][Tf_2N], we posit that the electrostatic attraction between solute R6G cation and solvent anion [Tf_2N] is the primary reason for the near-stick rotational behavior of R6G in [C_4mpyr][Tf_2N].

Our assertion of a specific solute−solvent interaction in R6G/[C_4mpyr][Tf_2N] is not without precedent. This topic has been subject to considerable scrutiny in the past few years. Dutt's group compared the rotational dynamics of nonpolar 9-phenylanthracene (9-PA) and polar charged rhodamine 110 (R110) in 1-butyl-3-methylimidazolium hexafluorophosphate ([C_4mim][PF_6]) and glycerol.[33] The reorientation times for 9-PA were longer in glycerol than in [C_4mim][PF_6] while the reorientation times of R110 were longer in [C_4mim][PF_6] than in glycerol. They found that the rotational dynamics of nonpolar 9-PA can be reasonably explained by considering the difference in molecular size through eq 4 but the slower rotational dynamics of R110 in [C_4mim][PF_6] are due to the stronger solute−solvent hydrogen bonds. On the other hand, when they changed the anion of the ionic liquids to tris(pentafluoroethyl)trifluorophosphate (FAP), the rotational dynamics of R110 in [C_4mim][FAP] was still close to the stick boundary condition. This was attributed to specific interactions between the cationic solute and the FAP anion in the RTILs. Superstick behavior was also demonstrated by Fruchey and Fayer[21] using a trianion sodium 8-methoxypyrene-1,3,6-sulfonate (MPTS). The observed friction coefficient C_{obs} was reported to be 2.22, 2.36, and 2.77 for the homologous series [$C_n$mim][Tf_2N], with n = 2, 4, and 6, respectively. After analysis using SED hydrodynamic theory and the Nee-Zwanzig dielectric friction model, they concluded that the motion of MPTS in ionic liquids was strongly hindered by RTIL cations that were strongly bound to the sulfonate anion. However, the dielectric friction model alone cannot explain the superstick

dx.doi.org/10.1021/jp303186v | J. Phys. Chem. B 2012, 116, 7883−7890

behavior of MPTS. They attributed the superstick behavior at least partially to the "solventberg" effect, where association of a large solvent molecule with the rotating solute molecule effectively increases the hydrodynamic volume and therefore slows down the rotational dynamics. The same argument can be also used to explain the near-stick behavior observed in this study. A similar solvent-adduct argument was made in earlier work to explain the temperature-dependent dynamics of the fluorescent rotor *N,N′*-bis(2,5-ditert-butylphenyl)-3,4,9,10-perylenedicarboximide (BTBP) within the RTIL 1-butyl-3-methylimidazolium hexafluorophosphate.[9]

Translational Dynamics Measured from NMR. The spectrum of 0.05 M R6G in $[C_4mpyr][Tf_2N]$ is shown in Figure 3. The assignments of the ^1H resonances of the RTIL

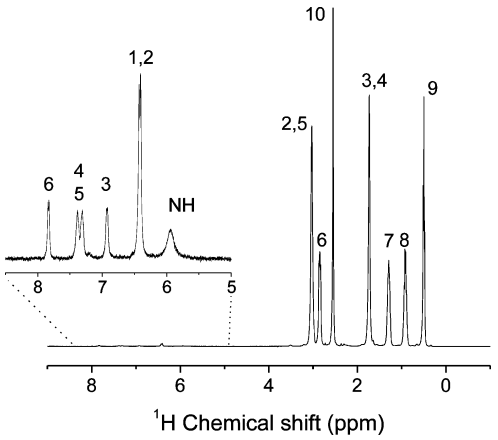

Figure 3. ^1H NMR spectrum of 0.05 M R6G in $[C_4mpyr][Tf_2N]$ recorded at 300 K. The resonance assignments in the spectrum correspond to the designations on the structures of Figure 1. The aromatic region (R6G signals) is replotted with a 64× vertical expansion with respect to the aliphatic region $[C_4mpyr]$ signals.

indicated on the aliphatic resonances between 0 and 3 ppm correspond to the designations on the structures of Figure 1. The resonances between ∼6 and 8 ppm, shown at a 64× vertical expansion, are the aromatic and NH peaks of R6G. Spectral assignments are indicated on the R6G formula of Figure 1. The ^1H resonances of the ethyl and methyl groups of R6G, are not well resolved from the intense RTIL resonances. In the PFG NMR method, diffusion coefficients are obtained by measuring the decrease in integrated intensity of a resonance in the spectrum of a molecule that arises from z axis translational motion of the molecule.[37] Any convenient resonance in the spectrum may be used for this purpose. Several resonances can be measured simultaneously to provide adequate statistics on the error in the measurements. Measurements of the diffusion coefficient for the solvent and solute were made concurrently. A second sample, 0.01 M in R6G, was also examined to assess the effect of solute dilution on D. Diffusion data collected over a 100 K temperature range are plotted in Figure 4. Data for solute and solvent, at both R6G concentrations, as well as the data for the neat solvent are shown.

Figure 4a is a plot of diffusion coefficients of R6G in $[C_4mpyr][Tf_2N]$ and of the neat $[C_4mpyr][Tf_2N]$ vs inverse temperature. The diffusion of the $[C_4mpyr]^+$ as a pure solvent and containing R6G in dilute concentrations are virtually identical and indicate that R6G concentrations ≤0.05 M do not have a measurable effect on solution viscosity. The diffusion coefficient of R6G is smaller than that for the $[C_4mpyr]^+$ cation, reflecting the larger hydrodynamic radius of the dye relative to the cation. The single data point represented by the star in Figure 4a is the R6G diffusion coefficient determined using FCS at 2×10^{-9} M.[49] It lies on the line extension from the NMR data, suggesting good agreement between the two methods even though the concentrations of R6G in RTIL are different by 7 orders of magnitude. Figure 4b plots D versus T/η. The linear responses from both $[C_4mpyr]$ and R6G obey the Stokes−Einstein relation for self-diffusion of liquids, $D = k_bT/6\pi\eta r_s$, where k_b is the Boltzmann constant, T is the absolute temperature, η is viscosity, and r_s is the hydrodynamic radius of the molecules.

Self-Reorientation of $[C_4mpyr][Tf_2N]$ Measured Using NMR. *^1H NMR.* The assumption of isotropic motion is explicit in the derivation of eq 2 and 3. Only spherically shaped

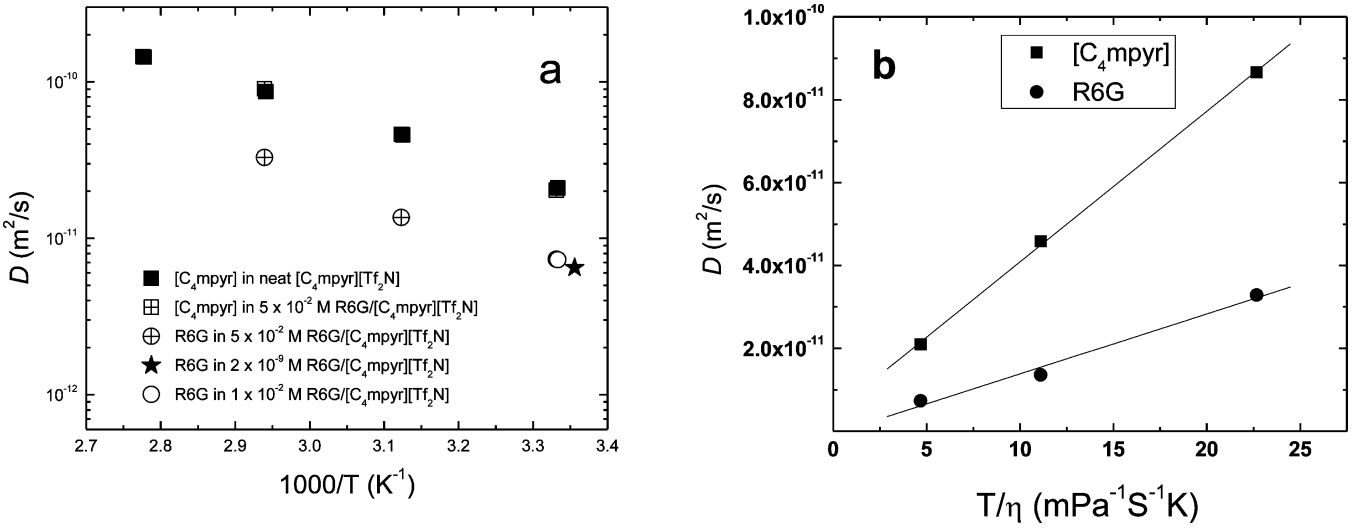

Figure 4. (a) Temperature dependence of the diffusion coefficient of R6G and $[C_4mpyr]^+$ in 0.01 and 0.05 M R6G/$[C_4mpyr][Tf_2N]$ and of $[C_4mpyr]^+$ in neat $[C_4mpyr][Tf_2N]$. The single data point represented as a star denotes the diffusion coefficient of R6G in 2×10^{-9} M R6G/$[C_4mpyr][Tf_2N]$ measured using FCS. (b) Diffusion coefficient plotted against T/η demonstrates the linear response expected from the Stokes−Einstein equation.

dx.doi.org/10.1021/jp303186v | J. Phys. Chem. B 2012, 116, 7883−7890

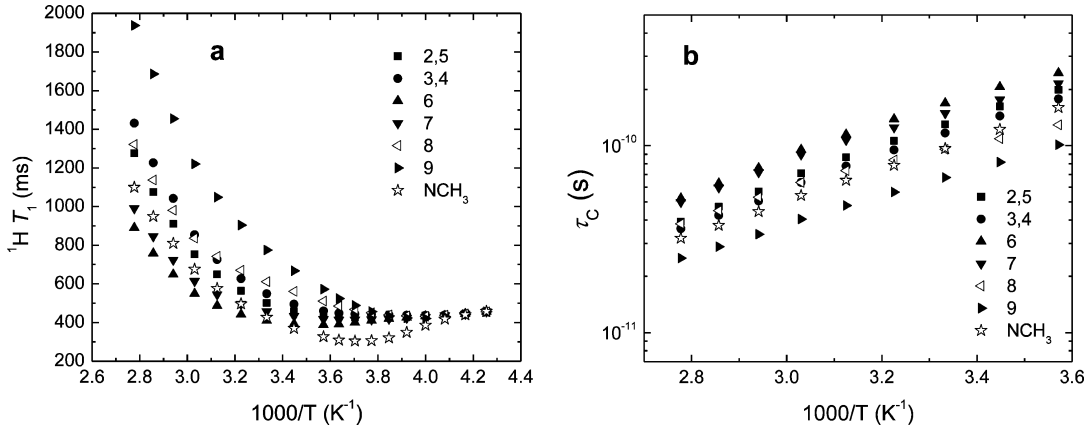

Figure 5. (a) Temperature dependence of ^{1}H T_1 of each of the sites of the cation [C_4mpyr] of [C_4mpyr] [Tf_2N]. (b) Temperature dependent correlation times for each site of the cation [C_4mpyr] of [C_4mpy][Tf_2N] calculated from the temperature dependence of ^{1}H T_1.

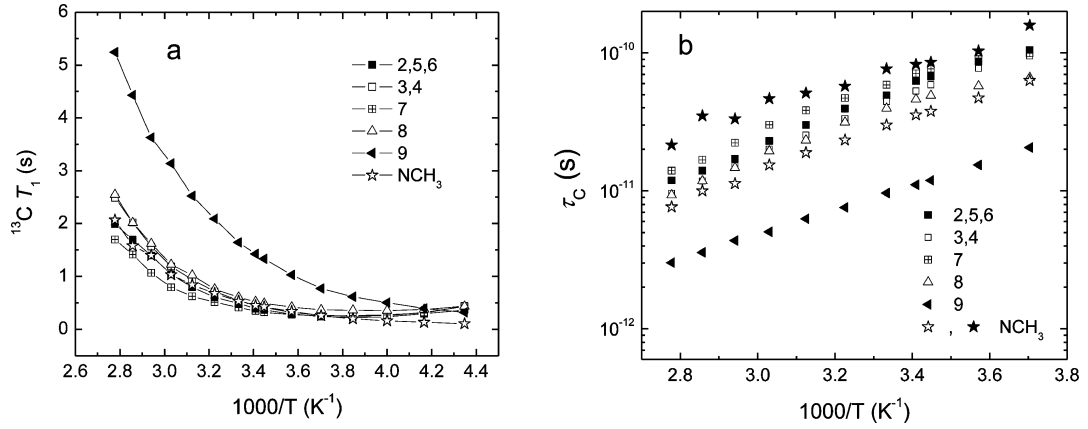

Figure 6. (a) Temperature dependent ^{13}C T_1 of each carbon site of the cation [C_4mpyr]. (b) Correlation times for each carbon site of the cation [C_4mpyr] vs inverse temperature. All values are τ_C except values indicated by the black stars which are τ_{NCH3}, the correlation time for methyl rotation about the N−C bond, calculated as $\tau_{NCH3}^{-1} = \tau_C^{-1} - \tau_R^{-1}$.

molecules strictly meet this condition and are completely characterized by a single correlation time. While the actual movement of molecules in solution can be complex, in many organic molecules with significant departures from spherical shape, the deviation from isotropic motion is not large. The τ_C in eq 2 (and 3) is understood as an effective correlation time representing the average time a molecule takes to rotate through one radian (2π rad/s = 1 rev/s). In addition to molecular reorientation, molecules may have multiple modes of internal motion, e.g., methyl group rotation, segmental motion along an alkyl side chain, isomerism and conformational ring inversions, among others. Each of these motions modulate the dipole−dipole interaction between coupled sites and can cause spin−lattice relaxation if the motion has a significant spectral density component at the Larmor frequency.

Figure 5a is a plot of the ^{1}H spin−lattice relaxation times vs inverse temperature for the individual proton resonances of [C_4mpyr][Tf_2N]. In this cation all protons except the two methyl groups are part of methylene sites and should experience similar T_1 if the overall motion of the molecule approximates isotropic behavior. This expectation relies on the short proton internuclear distance of geminal hydrogens (r_{gem} = 1.8 Å) that will dominate methylene proton relaxation. The methylene T_1 values, 0.49 ± 0.06 at 300 K, qualitatively support the notion of isotropic motion. Vicinal hydrogens (r_{vic} = 2.4 − 3.0 Å) and protons that may be spatially near by virtue of conformation, e.g., 1,6-hydrogen−hydrogen interactions, do make significant contributions to overall relaxation and contribute to the range of the methylene T_1s.

The N−CH_3 group T_1 is short. Figure 5a shows that the minimum N−CH_3 T_1 value (0.3 s) is shorter than all methylene T_1 minima (0.42 ± 0.03 s). In the limit of slow rotation ($\tau_C \ll \tau_{NCH3}$) the N−CH_3 T_{1min} is expected to be about 0.2 s based on the ring methylene values. Conversely, when $\tau_{NCH3} \ll \tau_C$, the T_1 will increase 4-fold.[50] The short T_1 signifies rotation about the N−CH_3 bond is comparable to the molecular reorientation time, a result shown explicitly in Figure 5b, a plot of effective correlation times for the protons of [C_4mpyr] vs inverse temperature.

^{13}C NMR. The temperature dependent ^{13}C T_1 and derived τ_C data for [C_4mpyr][Tf_2N] are summarized in Figure 6, panels a and b, respectively. At room temperature (300 K) the methylene carbons of the ring have T_1 values of 0.51 ± 0.02 s. This tight cluster of values validates the isotropic approximation and provides the correlation time for overall molecular reorientation of the ring, τ_R, through eq 3. Side chain segmental motion is apparent by the lengthening T_1s along the chain toward the methyl terminus. The correlation time plot (Figure 6b) depicts the effect of increased motion down the side chain toward the methyl group with the τ_C order: C(7) > C(8) > C(9). The chain end methyl shows a typical lengthened

dx.doi.org/10.1021/jp303186v | J. Phys. Chem. B 2012, 116, 7883−7890

T_1 (1.64 s) from rapid internal motion.[41] The N−CH_3 group has a T_1 of 0.53 s, similar to the ring methylene carbons.

This relaxation time is remarkably short and suggests the internal rotation rate of the CH_3 group about the C−N bond of the NCH_3 group is slow. When the NCH_3 rotational correlation time is greater than that of the ring reorientation time, $\tau_C \ll \tau_{NCH3}$, the internal methyl rotation will not contribute to methyl group relaxation. The T_1 for this "static" methyl group is then governed by overall molecular reorientation and the number of directly attached protons. Hence the NCH_3 T_1 will be 0.34 s [2/3(0.51)]. Conversely, in the limit of fast methyl group rotation the T_1 will be 9 times the "static" T_1 or 9(0.34) ≈ 3 s.[41] The N−CH_3 T_1 value is close to the T_1 predicted for the "static" limit.

In Figure 6b two values of τ for the N−CH_3 group are shown. That indicated by the unfilled star symbol is τ_C given by eq 3. The filled star symbol represents the internal N−CH_3 rotational correlation time, τ_{NCH3}, separated from the contribution due to molecular reorientation using the approximation[51]

$$1/\tau_c \approx 1/\tau_R + 1/\tau_{NCH3} \quad (8)$$

where τ_R is the overall molecular reorientation time, given by the ring carbon value. At this level of approximation, τ_{NCH3} indicates that the methyl rotation is slower than the ring reorientation by a factor of 2, compatible with the qualitative observations deduced from the T_1 values in Figure 6a.

The analysis of the rotational motion of [C_4mpyr][Tf_2N] by ^{1}H and ^{13}C NMR T_1 measurements convey the same qualitative information. The high viscosity of the RTIL means that overlap of the spin manifold and lattice motions occur on the ps time scale near room temperature and are readily studied by variable temperature NMR methods. [C_4mpyr][Tf_2N] is representative of many RTILs that contain a methyltrialkylammonium ion and an anion with delocalized charge. The N−CH_3 group in the cation displays slow rotation about the N−C bond as evidenced by correlation times for this motion that are typical of overall reorientation of the RTIL (10s to 100 ps). Our working hypothesis is that the long correlation times observed for NCH_3 rotation in these and other ILs is a general property of the local cation structure and displays "slow" rotation rates only in relation to the larger body of methyl rotation rates for methyl groups attached to carbon. In general, methyl groups attached to quaternary carbon centers have internal rotation times on the order of a few picoseconds,[41] in contrast to quaternary nitrogen sites (methyltrialkylammonium centers, structurally equivalent but charged), with rotation times longer by an order of magnitude. Our initial survey of N−CH_3 rotation rates in tetraalkylammonium salts (data to be published separately) show that slow N−CH_3 rotation is a common feature of these systems over diverse methyltrialkylammonium cation structures and for an array of both hard and soft anions. The CN bond is typically 4% shorter than the aliphatic CC bond distance. This general structural feature may be an important factor resulting in N−CH_3 rotational rates that are slower than analogous C−CH_3 rates.

CONCLUSION

In summary, we studied the diffusional and rotational dynamics of R6G in [C_4mpyr][Tf_2N] as well as self-diffusional and rotational dynamics of pure [C_4mpyr][Tf_2N] ionic liquid by combining time-resolved fluorescence anisotropy and NMR spectroscopy. The rotational dynamics of R6G in the pyrrolidinium RTIL are described by a near-stick boundary condition, which was attributed to the specific association of cationic R6G and anionic $[Tf_2N]^-$. The diffusion coefficients of R6G in the RTIL measured using ^{1}H NMR and florescence correlation spectroscopy (FCS) are the same in spite of the 10^7 fold difference in concentration used in those methods, suggesting both NMR and FCS can be used to rationalize the diffusion coefficients effectively and accurately. The correlation time for overall molecular reorientation of $[C_4mpyr]^+$ is shorter than the time for internal N-methyl group rotation, by about a factor of 2. The slow N−CH_3 rotation rates observed through both ^{1}H and ^{13}C NMR T_1 measurements were attributed to internal structure of the cation.

AUTHOR INFORMATION

Corresponding Author

*Tel: 865-574-4920. Fax: 865-574-8363. E-mail: shawrw@ornl.gov; hagamanew@ornl.gov.

Notes

The authors declare no competing financial interest.

ACKNOWLEDGMENTS

Research supported by the Fluid Interface Reactions, Structures, and Transport (FIRST) Center, an Energy Frontier Research Center funded by the U.S. Department of Energy, Office of Science, Office of Basic Energy Sciences (J.G., K.S.H., S.M.M., S.D., E.W.H., and R.W.S.) and by the Division of Chemical Sciences, Geosciences, and Biosciences, Office of Basic Energy Sciences, U.S. Department of Energy (G.A.B. and P.C.H.).

REFERENCES

(1) Castner, E. W., Jr.; Wishart, J. F. *J. Chem. Phys.* **2010**, *132*, 120901/1.
(2) MacFarlane, D. R.; Pringle, J. M.; Howlett, P. C.; Forsyth, M. *Phys. Chem. Chem. Phys.* **2010**, *12*, 1659.
(3) Wang, P.; Zakeeruddin, S. M.; Humphry-Baker, R.; Gratzel, M. *Chem. Mater.* **2004**, *16*, 2694.
(4) Kuang, D.; Wang, P.; Ito, S.; Zakeeruddin, S. M.; Gratzel, M. *J. Am. Chem. Soc.* **2006**, *128*, 7732.
(5) MacFarlane, D. R.; Huang, J.; Forsyth, M. *Nature* **1999**, *402*, 792.
(6) Han, X.; Armstrong, D. W. *Acc. Chem. Res.* **2007**, *40*, 1079.
(7) MacFarlane, D. R.; Forsyth, M.; Howlett, P. C.; Pringle, J. M.; Sun, J.; Annat, G.; Neil, W.; Izgorodina, E. I. *Acc. Chem. Res.* **2007**, *40*, 1165.
(8) Wishart, J. F. *Energy Environ. Sci.* **2009**, *2*, 956.
(9) Baker, S. N.; Baker, G. A.; Kane, M. A.; Bright, F. V. *J. Phys. Chem. B* **2001**, *105*, 9663.
(10) Baker, S. N.; Baker, G. A.; Munson, C. A.; Chen, F.; Bukowski, E. J.; Cartwright, A. N.; Bright, F. V. *Ind. Eng. Chem. Res.* **2003**, *42*, 6457.
(11) Shirota, H.; Funston, A. M.; Wishart, J. F.; Castner, E. W., Jr. *J. Chem. Phys.* **2005**, *122*, 184512.
(12) Shirota, H.; Wishart, J. F.; Castner, E. W., Jr. *J. Phys. Chem. B* **2007**, *111*, 4819.
(13) Ingram, J. A.; Moog, R. S.; Ito, N.; Biswas, R.; Maroncelli, M. *J. Phys. Chem. B* **2003**, *107*, 5926.
(14) Arzhantsev, S.; Jin, H.; Baker, G. A.; Maroncelli, M. *J. Phys. Chem. B* **2007**, *111*, 4978.
(15) Jin, H.; Baker, G. A.; Arzhantsev, S.; Dong, J.; Maroncelli, M. *J. Phys. Chem. B* **2007**, *111*, 7291.
(16) Mandal, P. K.; Samanta, A. *J. Phys. Chem. B* **2005**, *109*, 15172.
(17) Dey, S.; Adhikari, A.; Das, D. K.; Sasmal, D. K.; Bhattacharyya, K. *J. Phys. Chem. B* **2009**, *113*, 959.

(18) Chakrabarty, D.; Hazra, P.; Chakraborty, A.; Seth, D.; Sarkar, N. *Chem. Phys. Lett.* **2003**, *381*, 697.
(19) Chakrabarty, D.; Seth, D.; Chakraborty, A.; Sarkar, N. *J. Phys. Chem. B* **2005**, *109*, 5753.
(20) Sarkar, A.; Ali, M.; Baker, G. A.; Tetin, S. Y.; Ruan, Q.; Pandey, S. *J. Phys. Chem. B* **2009**, *113*, 3088.
(21) Fruchey, K.; Fayer, M. D. *J. Phys. Chem. B* **2010**, *114*, 2840.
(22) Dutt, G. B. *ChemPhysChem* **2005**, *6*, 413.
(23) Antony, J. H.; Dolle, A.; Mertens, D.; Wasserscheid, P.; Carper, W. R.; Wahlbeck, P. G. *J. Phys. Chem. A* **2005**, *109*, 6676.
(24) Borodin, O.; Gorecki, W.; Smith, G. D.; Armand, M. *J. Phys. Chem. B* **2010**, *114*, 6786.
(25) Endo, T.; Imanari, M.; Seki, H.; Nishikawa, K. *J. Phys. Chem. A* **2011**, *115*, 2999.
(26) Hayamizu, K.; Tsuzuki, S.; Seki, S. *J. Phys. Chem. A* **2008**, *112*, 12027.
(27) Imanari, M.; Uchida, K.-i.; Miyano, K.; Seki, H.; Nishikawa, K. *Phys. Chem. Chem. Phys.* **2010**, *12*, 2959.
(28) Damberg, P.; Jarvet, J.; Allard, P.; Mets, U.; Rigler, R.; Graslund, A. *Biophys. J.* **2002**, *83*, 2812.
(29) Millet, O.; Hudson, R. P.; Kay, L. E. *Proc. Natl. Acad. Sci. U.S.A.* **2003**, *100*, 12700.
(30) Dutt, G. B. *J. Phys. Chem. B* **2010**, *114*, 8971.
(31) Karve, L.; Dutt, G. B. *J. Phys. Chem. B* **2011**, *115*, 725.
(32) Khara, D. C.; Samanta, A. *Phys. Chem. Chem. Phys.* **2010**, *12*, 7671.
(33) Mali, K. S.; Dutt, G. B.; Mukherjee, T. *J. Chem. Phys.* **2008**, *128*, 054504/1.
(34) Ito, N.; Arzhantsev, S.; Maroncelli, M. *Chem. Phys. Lett.* **2004**, *396*, 83.
(35) Karve, L.; Dutt, G. B. *J. Phys. Chem. B* **2012**, *116*, 1824.
(36) Burrell, A. K.; Del, S. R. E.; Baker, S. N.; McCleskey, T. M.; Baker, G. A. *Green Chem.* **2007**, *9*, 449.
(37) JohnsonJr, C. S. *Prog. Nucl. Magn. Reson. Spectrosc.* **1999**, *34*, 203.
(38) Hayamizu, K.; Price, W. S. *J. Magn. Reson.* **2004**, *167*, 328.
(39) Fukushima, E.; Roeder, S. B. W. *Experimental Pulse NMR: A Nuts and Bolts Approach*; Addision-Wesley Publishing Company: Reading, MA, 1981.
(40) Abragam, A. *The Principles of Nuclear Magnetism*; Oxford University Press: New York, 1961.
(41) Allerhand, A.; Doddrell, D.; Komoroski, R. *J. Chem. Phys.* **1971**, *55*, 189.
(42) Das, S. K.; Sarkar, M. *J. Phys. Chem. B* **2012**, *116*, 194.
(43) Carlson, P. J.; Bose, S.; Armstrong, D. W.; Hawkins, T.; Gordon, M. S.; Petrich, J. W. *J. Phys. Chem. B* **2012**, *116*, 503.
(44) Funston, A. M.; Fadeeva, T. A.; Wishart, J. F.; Castner, E. W., Jr. *J. Phys. Chem. B* **2007**, *111*, 4963.
(45) Edward, J. T. *J. Chem. Educ.* **1970**, *47*, 261.
(46) Sension, R. J.; Hochstrasser, R. M. *J. Chem. Phys.* **1993**, *98*, 2490.
(47) Small, E. W.; Isenberg, I. *Biopolymers* **1977**, *16*, 1907.
(48) Jin, H.; O'Hare, B.; Dong, J.; Arzhantsev, S.; Baker, G. A.; Wishart, J. F.; Benesi, A. J.; Maroncelli, M. *J. Phys. Chem. B* **2008**, *112*, 81.
(49) Guo, J.; Baker, G. A.; Hillesheim, P. C.; Dai, S.; Shaw, R. W.; Mahurin, S. M. *Phys. Chem. Chem. Phys.* **2011**, *13*, 12395.
(50) Woessner, D. E. *J. Chem. Phys.* **1962**, *36*, 1.
(51) Doddrell, D.; Allerhan, A. *J. Am. Chem. Soc.* **1971**, *93*, 1558.